

# A novel method for measuring bowel motility and velocity with dynamic magnetic resonance imaging in two and three dimensions

David Willis<sup>1</sup>  | Donnie Cameron<sup>1,2</sup>  | Bahman Kasmai<sup>3</sup> |  
Vassilios S. Vassiliou<sup>1</sup>  | Paul N. Malcolm<sup>3</sup> | Gabriella Baio<sup>1,3</sup> 

<sup>1</sup>Norwich Medical School, University of East Anglia, Norwich, UK

<sup>2</sup>C. J. Gorter Center for High Field MRI, Department of Radiology, Leiden University Medical Center, Leiden, The Netherlands

<sup>3</sup>Department of Radiology, Norfolk & Norwich University Hospital NHS Trust, Norwich, UK

## Correspondence

David Willis, School of Environmental Sciences, University of East Anglia, Norwich, NR4 7TJ, UK.

Email: david.willis@uea.ac.uk

Increasingly, dynamic magnetic resonance imaging (MRI) has potential as a noninvasive and accessible tool for diagnosing and monitoring gastrointestinal motility in healthy and diseased bowel. However, current MRI methods of measuring bowel motility have limitations: requiring bowel preparation or long acquisition times; providing mainly surrogate measures of motion; and estimating bowel-wall movement in just two dimensions. In this proof-of-concept study we apply a method that provides a quantitative measure of motion within the bowel, in both two and three dimensions, using existing, vendor-implemented MRI pulse sequences with minimal bowel preparation. This method uses a minimised cost function to fit linear vectors in the spatial and temporal domains. It is sensitised to the spatial scale of the bowel and aims to address issues relating to the low signal-to-noise in high-temporal resolution dynamic MRI scans, previously compensated for by performing thick-slice (10-mm) two-dimensional (2D) coronal scans. We applied both 2D and three-dimensional (3D) scanning protocols in two healthy volunteers. For 2D scanning, analysis yielded bi-modal velocity peaks, with a mean antegrade motion of 5.5 mm/s and an additional peak at  $\sim 9$  mm/s corresponding to longitudinal peristalsis, as supported by intraoperative data from the literature. Furthermore, 3D scans indicated a mean forward motion of 4.7 mm/s, and degrees of antegrade and retrograde motion were also established. These measures show promise for the noninvasive assessment of bowel motility, and have the potential to be tuned to particular regions of interest and behaviours within the bowel.

## KEYWORDS

bowel dysmotility, Crohn's disease, dynamic MRI, gastrointestinal motility, quantification techniques

**Abbreviations used:** bSSFP, balanced steady-state free-precession; ECG, electrocardiogram; IBS, irritable bowel syndrome; RMS, root mean square; TRICKS, Time Resolved Imaging of Contrast Kinetics.

This is an open access article under the terms of the Creative Commons Attribution License, which permits use, distribution and reproduction in any medium, provided the original work is properly cited.

© 2021 The Authors. *NMR in Biomedicine* published by John Wiley & Sons Ltd.

## 1 | INTRODUCTION

Bowel motility disorders can arise from several conditions and affect patients to varying degrees across a wide demographic. Inflammatory bowel conditions, such as Crohn's disease<sup>1</sup> and ulcerative colitis,<sup>2</sup> are often associated with bowel motility disorders.<sup>3</sup> Crohn's disease affects growth in children,<sup>4</sup> and has serious long-term implications, while ulcerative colitis is associated with a high risk of colon cancer.<sup>5</sup> Globally these two conditions affect more than 11 million people,<sup>6</sup> with the causes being poorly understood. Irritable bowel syndrome (IBS) is another type of functional gastrointestinal disease that affects 10%–15% of people in the developed world.<sup>7</sup> It is associated with bowel dysmotility but, crucially, it demonstrates no structural changes detectable by current routine diagnostic tools.<sup>8</sup> Causes of IBS range from psychological stress<sup>9</sup> to bacterial aetiology<sup>10</sup> and vitamin deficiency.<sup>11</sup>

Treatment options for the aforementioned disorders differ per condition and depend on the degree of symptoms. Examples include lifestyle changes, medication, and surgery.<sup>12</sup> However, as the incidence of conditions such as Crohn's disease increases, elective surgery is becoming commonplace to allay long-term effects.<sup>13</sup> To improve treatment of these illnesses and to develop our understanding of underlying conditions (as well as areas like drug delivery), it is vital that we develop quantitative means of discriminating pathological and healthy bowel segments.

Magnetic resonance imaging (MRI) is an ideal noninvasive tool for imaging the gastrointestinal tract due to its exceptional soft-tissue contrast. In studying both peristalsis and laminar flow in the bowel the noninvasive nature of MRI offers a safer alternative to barium-enemas,<sup>14,15</sup> x-ray investigations, and intraoperative assessment<sup>16</sup>; and, crucially, the current reference standard for bowel motility assessment, antroduodenal manometry, cannot measure flow. A number of MRI approaches exist, as reviewed by de Jonge et al.,<sup>17</sup> including tagging<sup>18,19</sup> and displacement mapping<sup>20</sup>; however, scan times can be long, with coarse temporal resolution, and some methods provide only surrogate measures. Some manual<sup>21</sup> and semiautomated<sup>22</sup> MRI methods give meaningful bowel motility metrics, but these can be labour-intensive and can require bowel preparation. Several recent reviews<sup>17,23,24</sup> have made a case for the development of quantitative and noninvasive measures of bowel function. However, MRI measures of bowel motility and transit are challenging, being subject to many of the same limitations as cardiac MRI methods,<sup>25</sup> and there are obstacles to the widespread adoption of these techniques. First, most approaches to date have been applied to two-dimensional (2D) data, leading to erroneous measurements as the bowel moves in and out of the 2D slice; this is a reason to move to three-dimensional (3D) imaging. Further, bowel motion occurs over a range of different spatial and temporal scales, and imaging protocols need to be optimised accordingly.<sup>26</sup> Indeed, protocols must be adapted to focus on specific bowel regions and time scales to obtain clinically useful measurements. Another consideration is that bowel preparation using oral contrast agents, while useful for distending the bowel and inducing wall motion that can be studied by MRI, may lead to nonphysiological motility patterns, and thus there is demand for methods that can be used both with and without such preparations.

In this proof-of-concept study we introduce a novel technique that is sensitive to flow within the bowel and is complementary to existing MRI protocols. It consists of a dynamic MRI acquisition that requires minimal bowel preparation (a 6-h fast) and can be applied using off-the-shelf 2D or 3D cine imaging pulse sequences. The subsequent image analysis supplies useful metrics for quantitatively assessing flow in bowel loops, and gives measures of laminar flow and peristaltic motion in standard units (mm/s). Here, we demonstrate this method in healthy volunteers and verify the results against invasive intraoperative measures from the literature.

## 2 | THEORY

Motility measures are concerned with capturing peristaltic motion in the bowel, where peristalsis is the contraction and relaxation of smooth muscle in the bowel wall, propagating in a wave in an antegrade direction. Such waves propel material, which flows in a laminar fashion due to its high viscosity. Measures of this laminar flow can be used to assess the bulk motion within the bowel. The function of the bowel can be characterised by the amplitude and propagation of peristaltic contractions, and how these translate to antegrade and retrograde flow. Previous work has looked at local measures of signal intensity variation,<sup>27</sup> or area change, within the small bowel, but not at the quantitative tracking of flow within the lumen,<sup>28</sup> with the exception of Hoad et al., who studied flow in the colon.<sup>29</sup> Therefore, new approaches that measure the degree of motion with respect to the vector described by the bowel are of great interest.

As shown in Figure 1, motion can be cylindrically integrated over  $\varphi$  and measured in terms of  $\alpha$ , allowing detection of contraction, translocation, and peristalsis in the bowel. However, any rotational information will be lost. Defining motion with respect to the long axis,  $\mathbf{b}$ , allows complex motion to be interpreted more easily. Furthermore, any signal of motion is summed over  $\varphi$ , increasing its significance in this inherently noisy technique.

The motion assessment method introduced here uses cost-function minimisation, the value of which determines how well motion has been detected, and the parameters used in the function determine the velocity. Spatially adjacent voxels in the image are sequentially fitted in the indirect time domain or 'motion domain'. All possible vectors are fitted, and previous minimisation results in surrounding voxels are overwritten if a better result is obtained. Consider  $a$  as a list of points or voxels,  $p$ , corresponding to the vector  $\mathbf{a}$  in Figure 1:

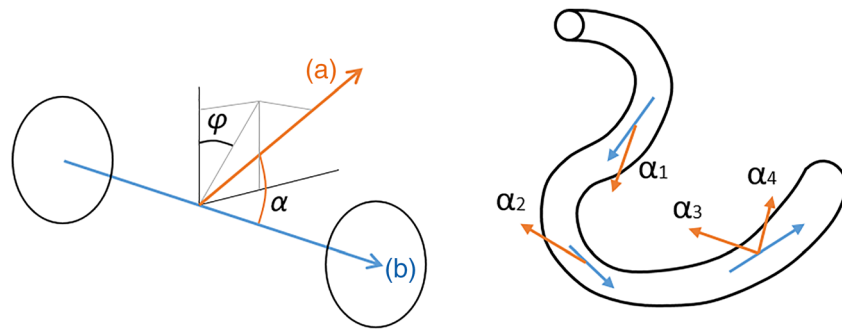


**FIGURE 1** The relationship of two vectors (left): **a**, a signal of motion; and the bowel direction, **b**. These give a value of  $\alpha$  via the dot-product. Vectors are summed over  $\varphi$  and the relationship with  $\alpha$  is obtained with increased signal, assuming cylindrical symmetry. For a given loop of bowel (right), dominant values for  $\alpha$  are assessed for regions of antegrade ( $\alpha_1$ ), retrograde ( $\alpha_2$ ), or mixed motion ( $\alpha_3$  and  $\alpha_4$ )

$$\mathbf{a} = \{p_0, p_1, p_2 \dots p_n\}, \quad (1)$$

where the number of voxels,  $n$ , determines the ‘lengthscale’ of the fit. Each voxel,  $p$ , has a spatial position and an associated time series:

$$p_n = x, y, z, \{\Delta S_t, \Delta S_{t+1}, \Delta S_{t+2} \dots \Delta S_{t+T}\}, \quad (2)$$

where  $\Delta S_t$  is the relative signal at a given time point,  $t$ , and  $T$  is the total acquisition time. A time shift,  $\Delta t$ , is nominally applied to the first adjacent voxel at the next time point, as material is assumed to have moved to this voxel. This  $\Delta t$  is then scaled to subsequent adjacent voxels ( $\Delta t'$ ) to give the signal,  $\Delta S_{t+\Delta t'}$ , as the same material is assumed to pass through each point. The mean signal can then be defined as:

$$\overline{\Delta S_{t+\Delta t}} = \frac{\sum_n (\Delta S_{t+\Delta t'})}{n}. \quad (3)$$

The mean-squared difference at each time point, relative to the mean signal, is given as:

$$m_{t+\Delta t} = \frac{\sum_n ((\Delta S_{t+\Delta t'})_i - \overline{\Delta S_{t+\Delta t}})^2}{n}. \quad (4)$$

The cost function,  $A$ , is then defined as:

$$A = \sqrt{\frac{\sum_T (m_{t+\Delta t})}{T}}. \quad (5)$$

The minimised  $\Delta t$  is then used to calculate the scalar component for velocity,  $v$ :

$$v_a = \frac{\overline{\Delta d_{xyz}}}{\Delta t_{\min(A)}}, \quad (6)$$

where the vector component is defined by the vector **a**.

Minimising cost functions where noise is a major component can cause algorithms to settle either where the noise is the lowest, or where the number of points is small (hence lower noise). Therefore, the algorithm minimising  $A$  is normalised by both the root mean square (RMS) of the whole time series, at  $p_0$ , and the number of points included in the minimisation. Further, values for  $\Delta t$  are only included in the minimisation of  $A$  if all voxels can contribute; if motion is too slow to encompass all points for a given  $\Delta t$ , minimisation is not performed. Minimisation of  $A$  should then settle on a  $\Delta t$  (and thus a  $v$ ) for which a velocity is present.

### 3 | MATERIALS AND METHODS

#### 3.1 | Simulations

To demonstrate our approach and the contributions of noise and the relative signal of the motion to our results, a set of 2D synthetic time series data was generated. The simulation was structured as a three-level intensity image of bright circles within an envelope, where each timeframe advanced the structure by two pixels.

A matrix of simulated images, with varying contrast and noise, was fed through the pipeline described above. Contrast levels between background and simulated bowel ranged from 0.2 to 0.9, and relative noise was introduced with standard deviations ranging from 1% to 50%.

#### 3.2 | MRI

Two healthy male participants (aged 31 and 37 years) were recruited. Each participant received a comprehensive description of the study, including possible risks, and gave informed consent according to the local ethics guidelines. Both participants were asked to fast for 6 h prior to the scan, and no oral contrast was used in order to maintain normal bowel reflexes. Scans were performed with participants in head-first supine orientation.

##### 3.2.1 | Bowel imaging in two dimensions

In 2011, two-dimensional bowel scans were acquired in the 31-year-old participant as part of work carried out by Farghal et al.<sup>27</sup> The scans were performed on a 1.5-T Avanto MRI scanner (Siemens Healthcare, Erlangen, Germany) using two flexible six-element anterior body matrix coils for signal reception. The whole abdomen was covered using 10 single-slice scans, acquired using a dynamic 'True FISP' balanced steady-state free precession (bSSFP) sequence with the following scan parameters: repetition time (TR) = 2.9 ms, echo time (TE) = 1.21 ms, flip angle = 80°, field of view (FOV) = 40 × 40 cm, matrix size = 192 × 118, slice thickness = 10 mm, in-plane resolution = 2.08 × 2.08 mm, partial Fourier factor = 0.75 in  $k_y$ , and temporal resolution = 964 ms. A total of 20 dynamic bSSFP images were acquired per slice, with prospective electrocardiogram (ECG) triggering, and each slice was acquired during a breath-hold of 19 s. Reproducibility of 2D imaging was assessed via 10 sequential 2D scans acquired in the same position in the same participant.

##### 3.2.2 | Bowel imaging in three dimensions

In 2019, three-dimensional bowel scans were obtained in the 37-year-old participant using a 3-T Discovery 750w MRI system (GE Healthcare, Milwaukee, WI, USA) with the combination of a flexible 12-channel anterior torso array and a 12-channel built-in posterior array for signal reception. We chose to use this system in order to access the fine-temporal-resolution Time Resolved Imaging of Contrast KineticS (TRICKS)<sup>30</sup> gradient recalled echo sequence, originally designed for angiography. Scans covered the whole abdomen from left to right, with a depth (anterior-posterior) of 44.8 mm, and were applied with the following parameters: TR = 2.0 ms, TE = 1.1 ms, flip angle = 5°, section thickness = 1.4 mm, in-plane resolution = 1.72 × 1.72 mm, FOV = 44 × 44 cm, matrix size = 256 × 256, radial partial Fourier factor = 0.5, ASSET factor = 2 (coil sensitivity-based acceleration), and true temporal resolution = 692 ms. A total of 35 dynamic images were acquired during a single breath-hold of ~ 20 s. The TRICKS baseline scan, which is intended as a precontrast scan for contrast-enhanced acquisitions, was discarded.

#### 3.3 | Image analysis

Bespoke code was written in Python (version 3.5.2) using Nibabel (v. 2.3.3) for image handling and Scipy (v. 1.3.0) libraries for fitting.

To highlight motion on the spatial scales of the bowel, each slice or section of the acquired imaging data was Fourier-filtered in the spatial domain for each time point using a dual Gaussian filter with  $\sigma_{\text{inner}} = 13$  and  $\sigma_{\text{outer}} = 50$ , masking structures both larger and smaller than the bowel. The filter was broad enough to preserve bowel signal for the small and large intestines and for size changes relating to motility. Also, structured noise or off-resonance artefacts such as Moiré fringes were minimised using this filter. A relative difference image was then calculated for each time point. Figure 2 shows an example of the preprocessing steps. Note that, in this case, the first time point of the 2D bSSFP acquisition had not yet reached equilibrium, thus this time point was dropped and subsequent slices were normalised to the median signal intensity of each image before preprocessing. It is worth noting that off-resonance banding artefacts in bSSFP can act to highlight motion when difference maps are used, as we do here.

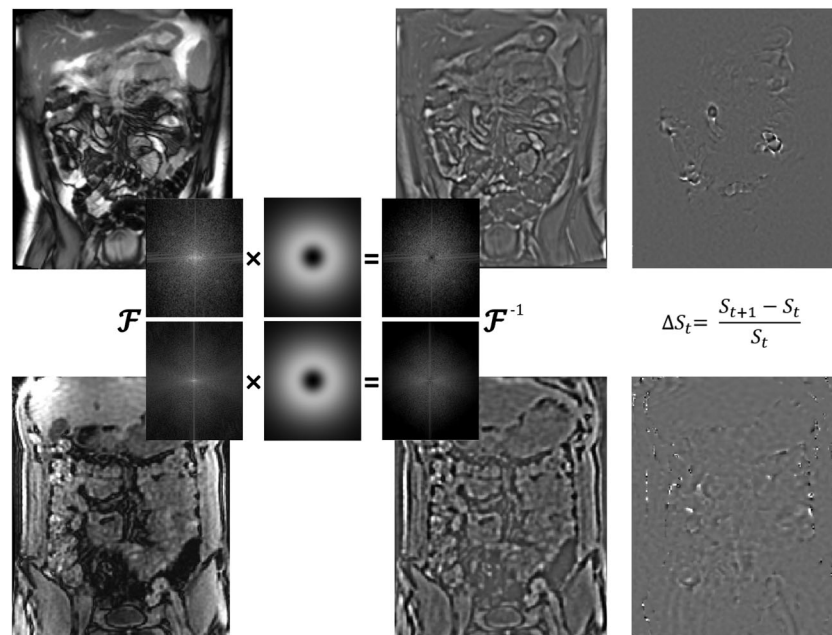


**FIGURE 2** An example of the preprocessing steps for: (top row) a 2D balanced steady-state free-precession (bSSFP) imaging sequence (2-mm in-plane resolution, 10-mm slice thickness, matrix size =  $156 \times 192$ ); and (bottom row) a 3D gradient recalled echo imaging sequence (1.72-mm in-plane resolution, 1.4-mm section thickness, matrix size =  $256 \times 256$ ). From left to right: the original acquisitions; their Fourier transforms; a dual Gaussian filter with  $\sigma_{\text{inner}} = 13$  and  $\sigma_{\text{outer}} = 50$ ; the Fourier-filtered data; the inverse Fourier transform of the filtered data; and the resulting difference map for each frame of the image

### 3.3.1 | Region-of-interest and vector delineation

Regions of interest were identified visually as regions of apparent motion on the cine scans, including a segment of transverse colon, terminating at the splenic flexure, as well as portions of the left colon, sigmoid colon, and right colon/caecum. Where possible, multiple adjacent regions from within the same bowel loop were summed to increase signal. Within each region, vectors,  $\mathbf{b}$ , were manually defined using the anatomical direction of the bowel loop by a Medical Physicist (D.W.) with 12 years of experience in contouring anatomy on CT and MR images, and a Consultant Radiologist (G.B.) with 17 years of radiology experience.

### 3.3.2 | Vector fitting

During the minimisation stage, starting values for  $\mathbf{A}$  (Equation 5) were initialised using a bounded basin-hopping approach, after which the cost function was minimised using a limited-memory BFGS algorithm. The vector fitting is of similar scale to the voxel sizes, hence not all respective angles of  $\mathbf{a}$  can be sampled for a given vector  $\mathbf{b}$ . Thus a relative weighting of each angle  $\alpha$  was calculated from each sample, based on the availability of pixels at different values of  $\varphi$ . Motions were visually assessed via 2D histograms showing velocity versus the direction of motion,  $\alpha$ . These were scaled to the total number of fitted vectors so that signals of motion appeared as discrete clusters of dark pixels. In general, vectors with  $\alpha$  in the range  $0-90^\circ$  were considered as demonstrating antegrade motion, while those with  $\alpha$  in the range  $90-180^\circ$  were considered retrograde.

Variability maps were also generated using the value of the minimised cost function,  $\mathbf{A}$  (Equation 5), and the RMS of the sequence in time. These are comparable with other methods currently used to assess bowel motility.

## 4 | RESULTS

### 4.1 | Simulations

Figure 3 relates our simulated example to the relationship seen in Figure 1. This simulation used a lengthscale of five pixels during the vector fit and the undersampling effect can be seen in the low contrast plot of Figure 3B. The expected result of this toy example is two pixels per time point, and the maps of velocity and direction converge on a single point for sufficiently high contrast and low noise. At low contrast, the motion

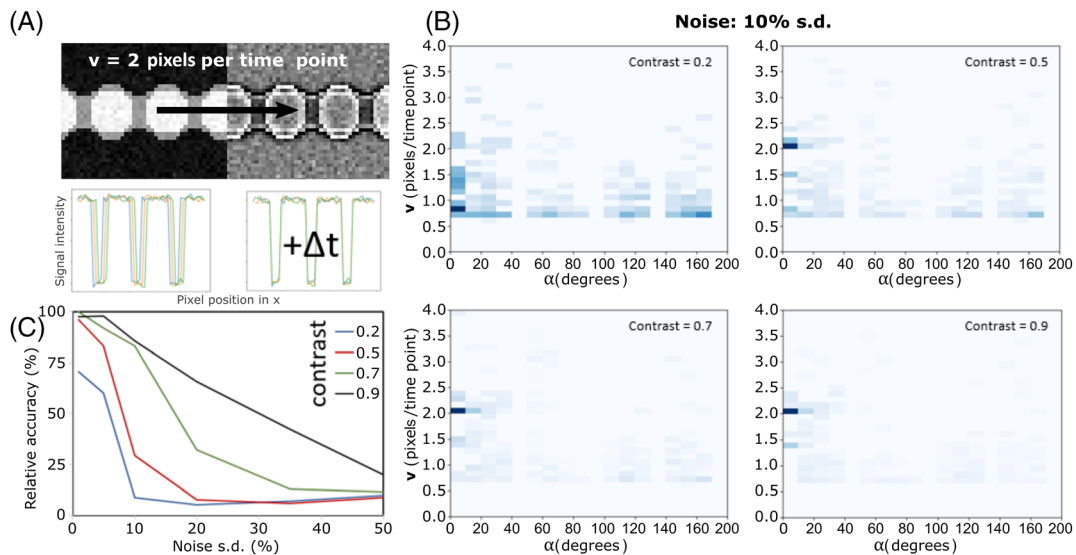


**FIGURE 3** (A) Simulated image data consisting of circles moving inside an envelope (relative contrast 0.8) at a rate of two pixels per time point. The left-hand panel shows the raw data, while the right-hand panel shows the Fourier-filtered data. (B) A selection of the outputs from the analysis pipeline for 10% relative noise and four contrast levels. Each plot is a 2D histogram of vectors fitted to the data in velocity,  $v$ , and direction relative to the anatomical direction of the simulated bowel,  $\alpha$  (in degrees). (C) A contrast-to-noise relationship is shown from the matrix of simulations, varying contrast and noise. The relative accuracy is calculated as the number of correct estimates of the known velocity/total number of velocities fit

signal is spread across all values for  $\alpha$ , but also tends to the lower limit for  $v$ . Therefore, the cost function will tend towards larger values of  $\Delta t$ , despite efforts to remove dependencies on regions of low RMS signal (in time) and reduced number of voxels used in the fit. This lower limit for  $v$  depends on the parameters of the scan and, in the case of 3D scanning, any anisotropy in the spatial resolution.

## 4.2 | Bowel imaging in two dimensions

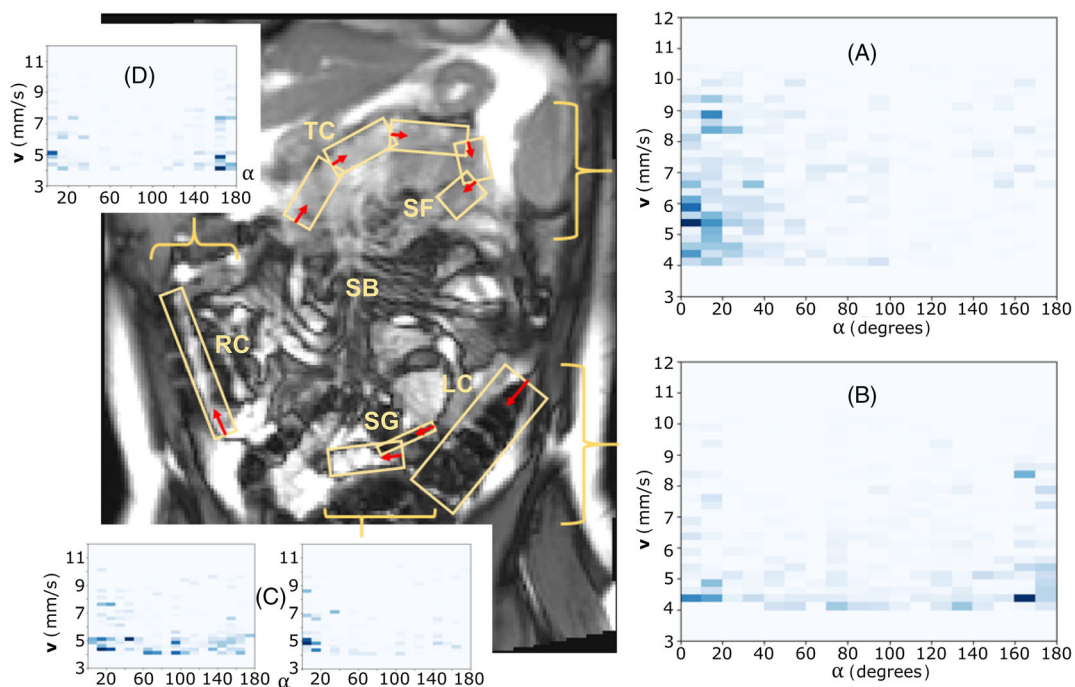
To speed up fitting and provide good coverage of the vectors overlaid on the image, the originating point for each vector was sequentially stepped over the image every third point; the lengthscale of the fit (namely, the number of voxels included in the vector,  $a$ ) was seven voxels; nine time points were included in the fit to allow for changes in motion over the course of the scan; and the process was repeated, stepping forwards in time by two time points.

Figure 4 shows the initial 2D image and selected regions where motion data were extracted. Region (A) is an area of bowel close to the stomach, with little content as a result of fasting; it shows forward motion in the loop bowel with a mean velocity of 6.6 mm/s. Region (B) is an area of large bowel and the magnitude of motion is small over the time scale of the scan, resulting in a small signal in the optimisation that tends towards the lower limit (in this case  $\Delta t$  was bounded to 0.5 in the fit, giving a lower limit for  $v$  of 4.16 mm/s). Regions (C) and (D) were selected to assess peristaltic velocities, as peristalsis was clearly visible on the cine images; however, partial volume effects in 2D data acquired from a thick slice introduce uncertainty, as the direction of motion relative to the angle of the slice is unknown. Region (C) is split into two volumes: one where bowel content and laminar flow can be separated (showing antegrade and retrograde flow); and a second that shows peristaltic motion (showing only antegrade flow). Finally, (D) is a region where the 2D slice does not bisect the centre of the bowel loop. It is worth noting that regions (C) and (D) may also demonstrate the presence of segmental contractions: either indirectly, in that they appear to show both antegrade ( $<90^\circ$ ) and retrograde ( $>90^\circ$ ) motion; or directly, as in region (C), where a signal of motion appears at  $\sim 90^\circ$ .

Figure 5 shows how the velocity profile from Figure 4A varies for different lengthscale profiles. The signal is persistent for the larger lengthscales but disappears when the lengthscale is reduced too far. Further, it can be seen that changing the lengthscale also alters the observed mean velocity, as the method is sensitised to different sources of motion.

### 4.2.1 | Reproducibility of 2D scans

When considering the reproducibility of the measure we must first consider how variable the motion may be in a given region of bowel. To look at variability over the 10 repeat scans, the loop of small bowel shown in Figure 4C was used, but with both regions defined by two values for  $b$  at



**FIGURE 4** Extraction of motion from nine positions in the 2D image shown on the left, where arrows represent the apparent direction of motion as visually determined from the cine image series. The x-axis of each 2D histogram is the angle between the vector the bowel describes and the vector of motion,  $\alpha$ . The y-axis is the velocity resulting from the minimised cost function, in mm/s. (A) A section of transverse colon (TC), terminating at the splenic flexure (SF), where the laminar flow is clearly visible to the eye as the images are animated; (B) A portion of the left colon with little apparent motion; (C) Sigmoid colon (SG) split into peristaltic wave (right) and some subsequent in/out plane motion; (D) A segment of right colon/caecum (RC), where the 10-mm 2D slice does not bisect the centre of the loop of bowel. SB, small bowel/mesentery root

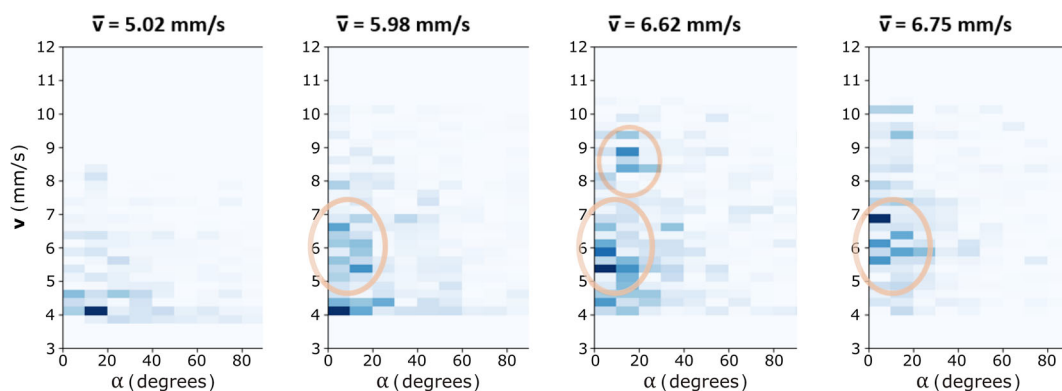


**FIGURE 5** A series of 2D histograms showing the variation of the signal in region (A) from Figure 4. The lengthscale (the nominal number of voxels used for each vector) of the optimisation was 3 (left), 5, 7, and 9 (right). The x-axis is restricted to the area with the highest signal. Above each plot is the mean velocity for all optimised vectors for that region. This value appears to change according to the lengthscale used, as the method becomes sensitised to different sources of motion. When considering different lengthscales the technique appears to be sensitive to up to two different signals of motion (circled), which may represent either laminar flow and peristalsis or cross-talk with adjacent bowel regions

the centre of the loop, and encompassing the whole width of the loop. The position of **b** was altered as the bowel moved between scans. The evolution can be seen in Figure 6, which shows 10 sequential 2D scans from the same participant. The initial scan shows a clear signal at 5.0 mm/s that is reproduced in approximately half of the subsequent scans. To give an indication of the forward and retrograde motion within that loop, Figure 7 shows the relative proportions of vectors representing antegrade ( $\alpha < 90^\circ$ ) and retrograde ( $\alpha > 90^\circ$ ) motion. The ratio of forward motion to retrograde motion ranges from 0.85 to 2.9. Combining the information in Figures 6 and 7 gives an indication of how the motion of the bowel changes over a longer time scale, with scans 7 and 8 showing notably more forward motion than retrograde.

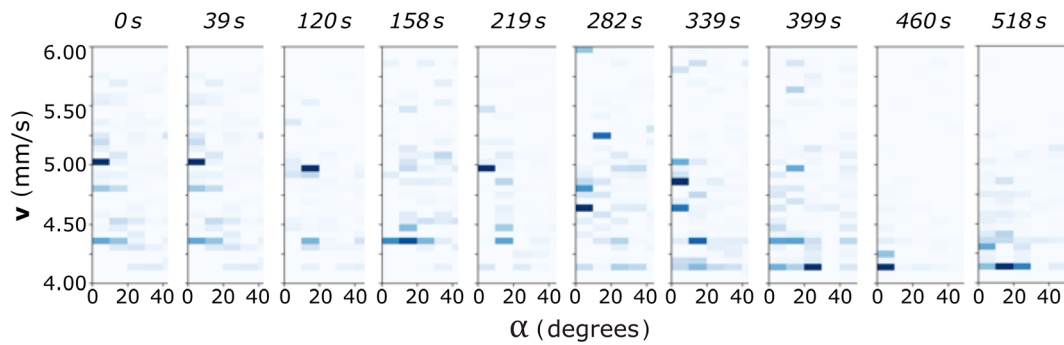


**FIGURE 6** A series of 2D histograms generated for 10 sequential scans, and analysed for the loop of bowel shown in Figure 4C. The measure was extended to the point where the bowel could be described by two vectors. The values for  $\alpha$  are restricted to the range 0–45° to highlight antegrade motion. For the second and fourth scans, a strong signal of retrograde motion was also observed at  $\sim 180^\circ$  (not shown)

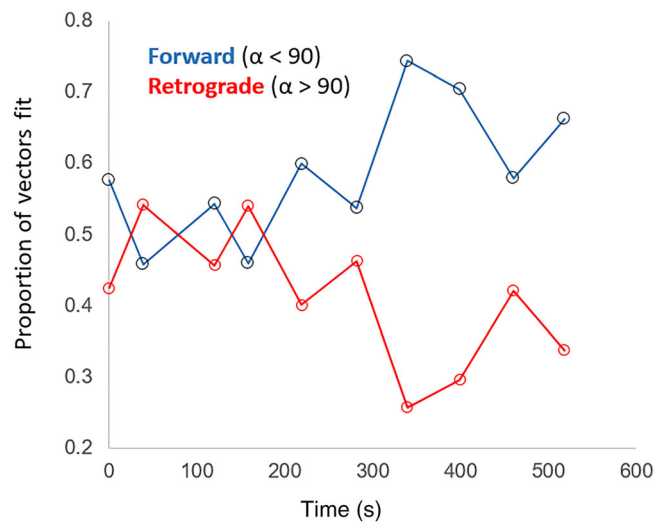


**FIGURE 7** The relative proportions of vectors contained within the cylindrical region of interest of the bowel, split by forward and retrograde motion. The time on the x-axis is the time at the beginning of each scan with respect to the initial scan

### 4.3 | Bowel imaging in three dimensions

Figure 8 shows an example of a 3D scan with some regions of motion extracted, allowing measures of motion that better correspond to the long axis of the bowel than for 2D scans. Trading the 10-mm coronal slice thickness in the 2D scan for a more isotropic voxel in the 3D scan, and maintaining comparable temporal resolution (2D: 964 ms; 3D: 692 ms), leads to lower signal-to-noise, but with an increase in the total number of voxels fitted within a given loop of bowel. This increase in the number of voxels makes the systematic noise of the technique more apparent and, in the case of the 3D scan, it is dictated by the relative scales of the image in the coronal and axial planes. The lower limit of the estimated velocity in the 3D case is therefore not as easily defined as the 2D case. The lengthscale was reduced to five voxels and seven time points, to reduce the effects of periodic noise in the acquired data. Reference data from the pylorus (Figure 8, blue) show a clear signal of motion at  $\alpha$  less than  $20^\circ$  with a mean velocity of 4 mm/s, whereas the mean forward ( $\alpha < 20^\circ$ ) velocities for the small bowel (Figure 8, green, red, and purple) are 4.5, 4.6, and 5.1 mm/s, respectively (mean: 4.7 mm/s). Note that the threshold of  $20^\circ$  for antegrade motion was chosen based on signals observed in the 2D data. Also shown are data from the liver, which is assumed to be stationary throughout imaging. The 2D histogram shows similar proportions of vectors across all angles, which represent the influence of noise. Further, most vectors are found in the range of velocities to which the analysis was sensitised, which was  $\sim 4$ –6 mm/s. In the pylorus and the bowel loops shown, these noisy vectors fade into the background due to relative scaling of the histograms, highlighting discrete signals of motion.

#### 4.3.1 | Variability maps

Figure 9 shows the averaged values of the minimised cost function and the RMS of the sequence in time.

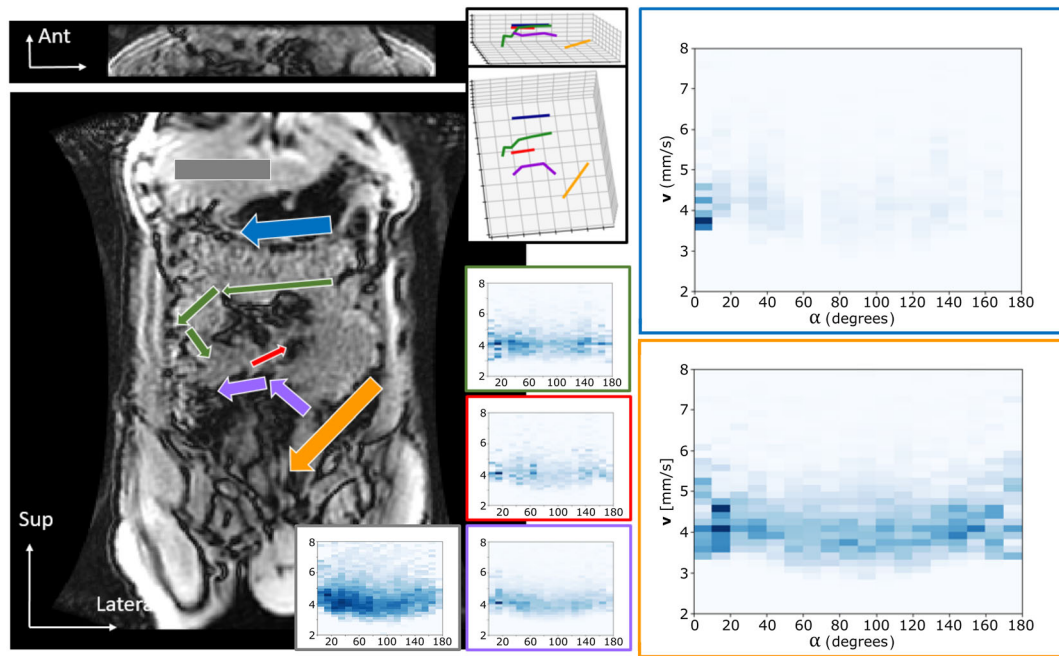


**FIGURE 8** Extraction of motion vectors from a 3D scan. Two slices are shown on the left with the vectors of motion inset, and approximate positions are shown with arrows for guidance. The corresponding 2D histograms for each region are shown on the right. Blue: peristalsis of the pylorus; orange: large bowel down to the sigmoid; green/red/purple: loops of small bowel with degrees of content from high to low. Also shown is a 2D histogram obtained from the liver (grey box), which can be used to illustrate the effect of noise, as the liver is assumed to be stationary. Note how the histogram appears homogeneously dark, across all angles, for the range of velocities to which this analysis was sensitised ( $\sim 4$ – $6$  mm/s). For motile structures such as the pylorus, and other bowel loops shown here, this noise fades to highlight clear and discrete signals of motion

## 5 | DISCUSSION

In this work we introduce a new method for quantifying bowel motility and velocity in two and three dimensions. The benefits of this method are as follows: (1) it provides a quantitative measure of motion within the bowel, as well as of the bowel itself; (2) it can be performed using off-the-shelf MRI sequences; (3) it can be applied in three dimensions to better track bowel anatomy; and (4) it complements existing surrogate measures in a manner that will enhance the field. Further, it is one of only a handful of approaches that have been applied with minimal bowel preparation, with others having been reported by de Jonge et al. and Khalaf et al.<sup>31,32</sup> The quantitative measure of velocity we obtain, along with the degree of antegrade or retrograde motion along the long axis of the looping bowel, permits the definition of expected laminar flow, provided there is sufficient image contrast between materials in the lumen. The information on retrograde motion we show here also has value: for example, when the ileocaecal valve is incontinent, as a result of surgery or an inflammatory condition such as Crohn's disease, retrograde motion can lead to large bowel bacteria colonising the small bowel. With our method we aim to bridge the diagnostic gap between the bowel's capacity to perform peristalsis and the impact this has on material moving through the digestive tract, helping to connect how motion then relates to absorption and related symptoms.

In addition to peristalsis and laminar flow, our method may also be capable of detecting segmentation contractions, a common type of mixing motility that is particularly apparent in the small bowel. The antegrade and retrograde signals of motion that we observe are indirect measures of bowel segmentation contractions and peristalsis, together. In theory, these segmentation contractions could be directly detected by our method, provided they are of a size and duration to which our scan is attuned. A specialised 'faster' sequence would detect smaller, faster segmentation contractions, for example. However, segmentation contractions can occur over both long and short time scales, both in close proximity to one another and far apart. Thus, the 3D acquisition we present here, with properly tuned time scales and lengthscales, would be required to adequately explore this phenomenon.

One area where our method has particular potential is for studying paediatric motility disorders.<sup>20</sup> The scan volumes for 3D acquisitions in children will likely be much smaller, permitting increased signal-to-noise, improved temporal resolution, and sensitivity to a wider range of velocities. However, limited breath-holding ability in younger patients might pose challenges for the detection of slower and longer time-scale periodic motions, and free-breathing acquisitions may be required to capture these. The current best available solution for bowel motility measurement is a displacement mapping approach, which is offered as a commercially available tool (Motilent, Ford, UK; <http://www.motilent.co.uk/>); however, this method is restricted to a 2D coronal slice. The main output measure is the degree of variation in the displacement, which reflects the

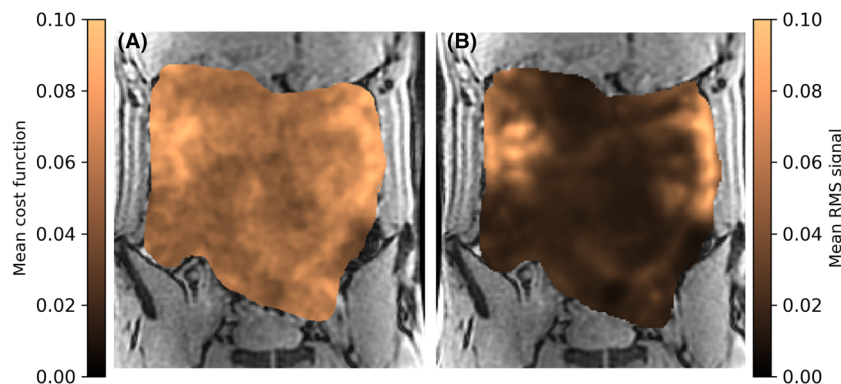


**FIGURE 9** (A) The mean cost function over time on a 3D scan, analogous to existing measures of bowel motility in two dimensions. Light areas are low values, indicating that motion is better detected. Loops of bowel are also clearly visible. Absolute values of this function range from 0.05 to 0.1; however, the absolute value will be highly dependent on the lengthscale of the fit and scanning parameters. (B) The mean root mean square (RMS) signal over time for the same section shown in (A)

contraction and peristalsis of the bowel; however, the flow within the bowel—anterograde or retrograde—is not considered in this approach. While this displacement mapping method provides measures for stratifying conditions like Crohn's disease, it has not been extended to 3D scanning in the 9 years since initial publication. Pure measures of variability show levels of activity,<sup>27</sup> but much is hidden in the third dimension. Although 3D scanning has been performed on the bowel<sup>33</sup> to achieve diagnostic quality images, the method introduced here does not require high-quality images to characterise motion. Moving to three dimensions reduces the signal, which manifests both as lower contrast-to-noise for the fitting (addressed to some extent by the method described here), and difficulty in delineating loops of bowel for applying a vector of measurement (i.e. the scans' utility as a visual tool). The advantage conversely is an order of magnitude increase in the number of voxels available when considering any vector of motion. The primary challenge, therefore, is in delineating the bowel region in which the motion is to be detected. In this study, only the 3D scans and their corresponding cost-function maps were used to determine bowel-containing motion (Figure 9A); however, in future studies a static high-contrast scan should be included to assist localisation.

In terms of published data, there are relatively few quantitative measures of peristaltic or laminar flow in the literature. A recent invasive study,<sup>16</sup> involving the intraoperative wrapping of the proximal jejunum with flexible printed circuit boards following a laparotomy procedure, measured wave-propagation patterns and a mean (SD) longitudinal velocity of 9.0 (0.7) mm/s. Circumferential velocity of the wave was seen to be faster at 10.8 (0.8) mm/s. For comparison, a histogram of forward motion ( $\alpha < 20^\circ$ ) for the region in Figure 4A can be seen in Figure 10, with the intraoperative result included. Our 3D scan data showed similar velocities (mean = 4.7 mm/s) in the small bowel, but no strong signal above 6 mm/s, suggesting laminar flow. However, the loop of bowel examined in Figure 4 is split bi-modally between a signal at 9 mm/s and a spread of velocities at around 5.5 mm/s. This suggests that both laminar flow and peristaltic flow are captured in our data. Previous MRI tagging work by Pritchard et al. obtained semiquantitative velocity data in the ascending colon,<sup>34</sup> showing simultaneous antegrade and retrograde flow, as well as complex flow in the hepatic flexure, and evidence of retrograde central 'jets' travelling in excess of 48 mm/s.

Regarding the varying spatial and temporal scales of bowel motion, the maximum detectable velocity is determined by the smallest value for  $\Delta t$ , so faster movement relies on the reliability of the fit when  $\Delta t$  is less than one time point, therefore encouraging finer timing resolution. It also follows that the minimum detectable velocity is governed by, variously: the number of voxels, the inverse of the number of time points, and the degree of overlap in time between the first and last voxels. The temporal scale (i.e. rate of change of motion) therefore imposes a trade-off with respect to the detectable velocities and the spatial scale that can be used. Scans should be maximised for signal-to-noise, but not at the expense of these considerations, to avoid the loss of important motion signals. In this study, we examined a relatively short period of bowel motion, due to breath-hold constraints of the healthy volunteers (~20 s), and our analysis largely focused on laminar flow. Clinical applications for this method are many—including chronic intestinal pseudo-obstruction,<sup>35</sup> Parkinson's disease,<sup>36</sup> and IBS<sup>37</sup>—and an extended free-breathing implementation of our approach could both confirm the initial measurements and provide information on longer time scales.<sup>38,39</sup> Figures 6 and 7 show how this motion evolves over repeated scans. However, due to the elastic nature of how peristalsis affects the bowel content, retrograde motion is also expected at a higher velocity,<sup>40</sup> and this was not seen. To capture these higher velocities, including the aforementioned retrograde central jets, requires a higher temporal resolution than was used in our study. Similarly, observing the generally slower moving large bowel requires either extending the lengthscale and the number of time points in the fit to the full extent of the 20-s breath-hold, or including sequentially acquired scans or free-breathing data in the analysis. We observed a small amount of motion in the large bowel; however, given the small signal in the bowel content in this case, any estimate of slow laminar flow is probably unreliable. Nevertheless, how this technique is applied is dictated by the area of clinical applicability, and thus we targeted, and successfully characterised, a broad middle ground of velocity profiles.

In this study we used product MRI pulse sequences made available by vendors. Given that our processing pipeline involved Fourier-filtering, a bespoke 3D sequence would be beneficial, as view-sharing in the TRICKS sequence is optimised for vascular scale detail in the centre of  $k$ -space

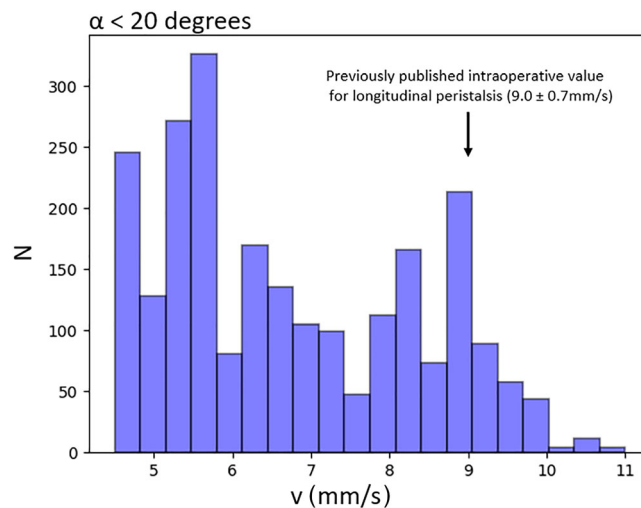


**FIGURE 10** A histogram of all velocities ( $\alpha < 20^\circ$ ) for the loop of bowel in the 2D scan described by Figure 4A. The arrow indicates the velocity of the longitudinal peristaltic wave measured in the jejunum intraoperatively<sup>16</sup>

that is ultimately filtered out in our method. The central region of the radially acquired  $k$ -space is repeatedly sampled (as per the specified trade-off between spatial and temporal resolution) alternately with annuli of  $k$ -space surrounding the centre. TRICKS divides  $k$ -space into four concentric regions (A-D, inner to outer) and samples in the order ABACAD, with the frame rate defined by the time between visits to the central region, which is filtered out in our approach. Altering the sampling scheme to regions BABC would avoid unnecessary detail loss and improve temporal resolution, which could be traded for greater signal-to-noise if desired.

In addition to developing a more specialised imaging sequence for our technique to optimise  $k$ -space filling, future work could focus on automated region of interest determination. Parallel computing could be used to fit every possible vector in the bowel, in all directions, and those that represent ‘true’ motion could be isolated using thresholding. From an applications perspective, the repeatability of our method should also be assessed in healthy volunteers and its results validated against the approach used by Motilent, which is routinely used in the clinical setting.

## 6 | CONCLUSION

We have shown in this work that it is possible to obtain linear measures of motion within the bowel in both two and three dimensions, and this can be achieved using product scanning sequences and minimal bowel preparation. This method provides a promising complementary tool for the noninvasive assessment of bowel motility, and has the potential to be tuned to particular bowel regions—such as the small bowel, large bowel, and ileocaecal sphincter—as well as to specific applications, including paediatric cases.

### ACKNOWLEDGEMENTS

The authors would like to thank Aser Farghal for collecting some of the initial data for this study.

### DATA AVAILABILITY STATEMENT

The data that support the findings of this study are available from the corresponding author upon reasonable request.

### ORCID

David Willis  <https://orcid.org/0000-0001-7183-7738>

Donnie Cameron  <https://orcid.org/0000-0001-9841-6909>

Vassilios S. Vassiliou  <https://orcid.org/0000-0002-4005-7752>

Gabriella Baio  <https://orcid.org/0000-0002-8397-5318>

### REFERENCES

1. Baumgart DC, Sandborn WJ. Crohn's disease. *Lancet*. 2012;380(9853):1590-1605.
2. Ford AC, Moayyedi P, Hanauer SB. Ulcerative colitis. *Br Med J*. 2013;346:f432. <https://doi.org/10.1136/bmj.f432>

3. Bassotti G, Antonelli E, Villanacci V, Salemme M, Coppola M, Annese V. Gastrointestinal motility disorders in inflammatory bowel diseases. *World J Gastroenterol*. 2014;20(1):37-44.
4. Beattie RM, Croft NM, Fell JM, Afzal NA, Heuschkel RB. Inflammatory bowel disease. *Arch Dis Child*. 2006;91(5):426-432.
5. Wanderås MH, Moum BA, Høivik ML, Hovde Ø. Predictive factors for a severe clinical course in ulcerative colitis: results from population-based studies. *World J Gastrointest Pharmacol Ther*. 2016;7(2):235-241.
6. GBD 2015 Disease and Injury Incidence and Prevalence Collaborators. Global, regional, and national incidence, prevalence, and years lived with disability for 310 diseases and injuries, 1990–2015: a systematic analysis for the Global Burden of Disease Study 2015. *Lancet*. 2016;388(10053):1545-1602.
7. Maxion-Bergemann S, Thielecke F, Abel F, Bergemann R. Costs of irritable bowel syndrome in the UK and US. *PharmacoEconomics*. 2006;24(1):21-37.
8. Enck P, Aziz Q, Barbara G, et al. Irritable bowel syndrome. *Nat Rev Dis Primers*. 2016;2:16014. <https://doi.org/10.1038/nrdp.2016.14>
9. Fukudo S, Nomura T, Muranaka M, Taguchi F. Brain-gut response to stress and cholinergic stimulation in irritable bowel syndrome. A preliminary study. *J Clin Gastroenterol*. 1993;17(2):133-141.
10. Ghoshal UC, Srivastava D. Irritable bowel syndrome and small intestinal bacterial overgrowth: meaningful association or unnecessary hype. *World J Gastroenterol*. 2014;20(10):2482-2491.
11. Williams CE, Williams EA, Corfe BM. Vitamin D status in irritable bowel syndrome and the impact of supplementation on symptoms: what do we know and what do we need to know? *Eur J Clin Nutr*. 2018;72(10):1358-1363.
12. Yeshi K, Ruscher R, Hunter L, Daly NL, Loukas A, Wangchuk P. Revisiting inflammatory bowel disease: pathology, treatments, challenges and emerging therapeutics including drug leads from natural products. *J Clin Med*. 2020;9(5):1273. <https://doi.org/10.3390/jcm9051273>
13. Amil-Dias J, Kolacek S, Turner D, et al. Surgical management of Crohn disease in children: guidelines from the Paediatric IBD Porto Group of ESPGHAN. *J Pediatr Gastroenterol Nutr*. 2017;64(5):818-835.
14. Bernstein CN, Boult I, Greenberg HM, Van der Putten W, Duffy G, Grahame GR. A prospective randomized comparison between small bowel enteroclysis and small bowel follow-through in Crohn's disease. *Gastroenterology*. 1997;113(2):390-398.
15. Toms AP, Barltrop A, Freeman AH. A prospective randomised study comparing enteroclysis with small bowel follow-through examinations in 244 patients. *Eur Radiol*. 2001;11(7):1155-1160.
16. Angeli T, O'Grady G, Vather R, Bissett I, Cheng L. Intra-operative high-resolution mapping of slow wave propagation in the human jejunum: Feasibility and initial results. *Neurogastroenterol Motil*. 2018;30(7):e13310. <https://doi.org/10.1111/nmo.13310>
17. de Jonge CS, Smout AJ, Nederveen AJ, Stoker J. Evaluation of gastrointestinal motility with MRI: advances, challenges and opportunities. *Neurogastroenterol Motil*. 2018;30(1):e13257. <https://doi.org/10.1111/nmo.13257>
18. Sprengers AM, van der Paardt MP, Zijta FM, et al. Use of continuously MR tagged imaging for automated motion assessment in the abdomen: a feasibility study. *J Magn Reson Imaging*. 2012;36(2):492-497.
19. de Jonge C, Sprengers A, Nederveen A, Stoker J. Spectral bowel motility assessment using dynamic tagged MRI. *Neurogastroenterol Motil*. 2017;29:43-44.
20. Menys A, Taylor SA, Emmanuel A, et al. Global small bowel motility: assessment with dynamic MR imaging. *Radiology*. 2013;269(2):443-450.
21. Wakamiya M, Furukawa A, Kanasaki S, Murata K. Assessment of small bowel motility function with cine-MRI using balanced steady-state free precession sequence. *J Magn Reson Imaging*. 2011;33(5):1235-1240.
22. Bickelhaupt S, Froehlich J, Cattin R, et al. Software-assisted quantitative analysis of small bowel motility compared to manual measurements. *Clin Radiol*. 2014;69(4):363-371.
23. Menys A, Saliakellis E, Borrelli O, Thapar N, Taylor S, Watson T. The evolution of magnetic resonance enterography in the assessment of motility disorders in children. *Eur J Radiol*. 2018;107:105-110.
24. Sulaiman S, Marciani L. MRI of the colon in the pharmaceutical field: the future before us. *Pharmaceutics*. 2019;11(4):146. <https://doi.org/10.3390/pharmaceutics11040146>
25. Hoad C, Clarke C, Marciani L, Graves MJ, Corsetti M. Will MRI of gastrointestinal function parallel the clinical success of cine cardiac MRI? *Brit J Radiol*. 2019;92(1093):20180433. <https://doi.org/10.1259/bjr.20180433>
26. de Jonge CS, Gollifer RM, Nederveen AJ, et al. Dynamic MRI for bowel motility imaging—how fast and how long? *Brit J Radiol*. 2018;91(1088):20170845. <https://doi.org/10.1259/bjr.20170845>
27. Farghal A, Kasmai B, Malcolm PN, Graves MJ, Toms AP. Developing a new measure of small bowel peristalsis with dynamic MR: a proof of concept study. *Acta Radiol*. 2012;53(6):593-600.
28. Odille F, Menys A, Ahmed A, Punwani S, Taylor SA, Atkinson D. Quantitative assessment of small bowel motility by nonrigid registration of dynamic MR images. *Magn Reson Med*. 2012;68(3):783-793.
29. Hoad C, Menys A, Garsed K, et al. Colon wall motility: comparison of novel quantitative semi-automatic measurements using cine MRI. *Neurogastroenterol Motil*. 2016;28(3):327-335.
30. Korosec FR, Frayne R, Grist TM, Mistretta CA. Time-resolved contrast-enhanced 3D MR angiography. *Magn Reson Med*. 1996;36(3):345-351.
31. de Jonge CS, Sprengers AM, van Rijn KL, Nederveen AJ, Stoker J. Assessment of fasted and fed gastrointestinal contraction frequencies in healthy subjects using continuously tagged MRI. *Neurogastroenterol Motil*. 2020;32(2):e13747. <https://doi.org/10.1111/nmo.13747>
32. Khalaf A, Nowak A, Menys A, et al. Cine MRI assessment of motility in the unprepared small bowel in the fasting and fed state: beyond the breath-hold. *Neurogastroenterol Motil*. 2019;31(1):e13466. <https://doi.org/10.1111/nmo.13466>
33. de Jonge C, Coolen B, Peper E, et al. Evaluation of compressed sensing MRI for accelerated bowel motility imaging. *Eur Radiol Exp*. 2019;3(1):1-12.
34. Pritchard SE, Paul J, Major G, et al. Assessment of motion of colonic contents in the human colon using MRI tagging. *Neurogastroenterol Motil*. 2017;29(9):e13091. <https://doi.org/10.1111/nmo.13091>
35. Fell J, Smith V, Milla P. Infantile chronic idiopathic intestinal pseudo-obstruction: the role of small intestinal manometry as a diagnostic tool and prognostic indicator. *Gut*. 1996;39(2):306-311.
36. Pfeiffer RF. Gastrointestinal, urological, and sexual dysfunction in Parkinson's disease. *Mov Disord*. 2010;25(S1):S94-S97.
37. Pimentel M, Soffer EE, Chow EJ, Kong Y, Lin HC. Lower frequency of MMC is found in IBS subjects with abnormal lactulose breath test, suggesting bacterial overgrowth. *Dig Dis Sci*. 2002;47(12):2639-2643.

38. Hamy V, Menys A, Helbren E, et al. Respiratory motion correction in dynamic-MRI: application to small bowel motility quantification during free breathing. *Med Image Comput Comput Assist Interv.* 2013;16(Pt 2):132-140.
39. Menys A, Hamy V, Makanyanga J, et al. Dual registration of abdominal motion for motility assessment in free-breathing data sets acquired using dynamic MRI. *Phys Med Biol.* 2014;59(16):4603-4619.
40. Schulze KS. The imaging and modelling of the physical processes involved in digestion and absorption. *Acta Physiol.* 2015;213(2):394-405.

**How to cite this article:** Willis D, Cameron D, Kasmai B, Vassiliou VS, Malcolm PN, Baio G. A novel method for measuring bowel motility and velocity with dynamic magnetic resonance imaging in two and three dimensions. *NMR in Biomedicine.* 2021;e4663.  
doi:10.1002/nbm.4663